Materials Science and Engineering, A118 (1989) 155–170

Reaustenitization Experiments on some High-strength Steel Weld Deposits

J. R. YANG

Taiwan National University, Department of Materials Engineering, Taipei (Taiwan)

H. K. D. H. BHADESHIA

University of Cambridge, Department of Materials Science and Metallurgy, Pembroke Street, Cambridge CB2 3QZ (U.K.)

(Received February 21, 1989)

Abstract

The kinetics of the reverse transformation from ferrite to austenite have been investigated to provide a basis for the modelling of microstructure in multirun, steel weld deposits. The reaustenitization process has been studied for two starting microstructures, one consisting of a mixture of bainitic ferrite and austenite, and the other of acicular ferrite and austenite. Both isothermal and continuous heating experiments have been carried out under conditions where reverse transformation involves simply the growth of already existing austenite. The results are analysed theoretically using an approximate model for the growth of austenite, and an attempt is made to explain the differences in the observed reaustenitization behaviour of bainite and acicular ferrite.

1. Introduction

A knowledge of the kinetics of austenite (γ) nucleation and growth is vital in understanding many of the common microstructures which arise in wrought and welded steels used commercially [1–9]. For example, any attempt at the prediction of microstructure in the heat-affected zones of steel welds, requires either a knowledge of, or a method of computing the time–temperature–transformation (TTT) diagram for the transformation of a specified initial microstructure into austenite. It would be necessary to have such information as a function of the average chemistry of the alloy and of the nature of the initial microstructure involved. The reaustenitization process can be sensitive to the details of the initial microstructure, details such as the phase chemistries, grain size, grain shape, etc. This contrasts with the usual transformation of austenite into ferrite (α), where the TTT diagrams are sensitive to just the amount of austenite grain boundary per unit volume, and the average steel chemistry.

A facility must also exist for converting the isothermal transformation diagrams into continuous-heating transformation (CHT) diagrams, since most industrial processes involve anisothermal heat treatments. During welding, regions of the parent plate and of the fusion zones of multirun welds undergo transient temperature rises which sometimes take the alloy into the $\alpha+\gamma$ phase field, causing profound changes in microstructure by the time the weld has cooled back to the ambient temperature.

Some of the key thermodynamic characteristics of the process of isothermal reaustenitization for steel weld deposits have already been reported [5, 6]. Those investigations dealt with the growth of austenite from two different initial microstructures, one consisting of a mixture of acicular ferrite and austenite ($\alpha_a+\gamma$) and the other of bainite and austenite ($\alpha_b+\gamma$). The present work attempts to deal with some aspects of the overall transformation *kinetics* of reaustenitization, using the same initial microstructures. The CHT behaviours of homogenized and heterogeneous weld metals are also investigated, although in a more limited way. The alloys used are a part of a programme for the design of better high-strength steel weld deposits [10–12]; a key aim in this programme is to design a multirun weld which is mechanically homogeneous while at the same time has high strength. This requires a detailed knowledge of the reaustenization process [10–12].

2. Experimental techniques

2.1. Alloys

Alloys 1–3 were deposited using manual metal arc welding (Table 1); the base plate is designated

0921-5093/89/$3.50

Alloy 4 in Table 1. The majority of experiments were conducted using Alloy 1, the remaining alloys being a part of another study of high-strength steel weld deposits. The electrodes (4 mm diameter) used were of a AWS-E10016-G type, the joint geometry being compatible with British Standard BS639 (similar to ISO2560), a geometry which gives large regions of weld metal free from dilution by the parent plate. The samples were all machined from regions not influenced by dilution. The welding was carried out in the flat position using the stringer bead technique, the parent plate thickness being 20 mm. The welding current and voltage used were 180 A 23 V (d.c.+) respectively, with an electrical energy input of about 2 kJ mm^{-1}, the weld consisting of some 27 runs with 3 runs per layer. The interpass temperature was typically 250 °C.

To mitigate any effect of alloying element segregation (*i.e.* the segregation which is a consequence of non-equilibrium solidification) on the kinetics of reaustenitization, some samples of all the weld deposits were homogenized at 1300 °C for 3 days, while sealed in quartz tubes containing pure argon. These samples are identified throughout the text by preceding the alloy designation with the letter "H" (*e.g.* Alloy H1).

2.2. Dilatometry

All kinetic measurements were performed on a Theta Industries high-speed dilatometer, which has a water cooled r.f. furnace of essentially zero thermal mass, since it is only the specimen which undergoes the programmed thermal cycle. This enables rapid heating or cooling experiments.

TABLE 1 Chemical compositions (in weight per cent). Alloys 1–3 are manual metal arc weld deposits, and Alloy 4 represents the composition of the base plate. The compositions were determined spectroscopically, except for oxygen and nitrogen, which were measured using Leco furnaces, with 50 g of material for each determination to ensure representative results

Alloy	*C*	*Si*	*Mn*	*Ni*	*Mo*	*Cr*	*V*
1	0.060	0.27	1.84	2.48	0.20	0.05	0.01
2	0.040	0.37	1.70	2.36	0.20	0.04	0.02
3	0.040	0.33	1.62	2.44	0.01	0.04	0.01
4	0.17	0.33	1.42				

	S	*P*	*Al*	*Ti*	*Nb*	*O*	*N*
1	0.005	0.012	0.01	0.02	0.01	0.0320	0.0111
2	0.008	0.015	0.02	0.03	0.01	0.0317	0.0098
3	0.008	0.014	0.02	0.02	0.01	0.0320	0.0107

The length transducer on the dilatometer was calibrated using pure platinum and pure nickel specimens of known thermal expansion characteristics. The dilatometer has been specially interfaced with a BBC/Acorn microcomputer so that length, time and temperature information can be recorded at microsecond intervals, and the data stored for further analysis.

Specimens for dilatometry were in the form of rods 3 mm in diameter and 15 mm in length, machined from the weld deposits with the cylinder axes parallel to the welding direction. The specimens were machined from regions far from the fusion line of the parent plate and are not affected by dilution from the parent material. To avoid surface nucleation and surface degradation, all specimens were electroplated with nickel (plating thickness approximately 0.08 mm) and all heat treatments were carried out in a helium gas environment.

2.3. Transmission electron microscopy

Thin foil specimens were prepared for transmission electron microscopy from disks 0.25 mm thick slit from specimens used in the dilatometric experiments. The discs were thinned to 0.05 mm by abrasion on silicon carbide paper and then electropolished in a twin jet electropolisher using a 5% perchloric acid, 25% glycerol and 70% ethanol mixture at ambient temperature and 60 V polishing potential. The microscopy was carried out using a Philips EM400T transmission electron microscope operated at 120 kV.

3. Results and discussion

3.1. Isothermal reaustenitization experiments

Recent work [5, 6] has examined the thermodynamics of isothermal reaustenitization from starting microstructures which are either mixtures of acicular ferrite and austenite, or of bainite and austenite. The bainite or acicular ferrite is first obtained by the partial isothermal transformation of austenite at a temperature T_a (less than B_s), and the resulting microstructure is then heated rapidly to a temperature T_γ to permit the growth of austenite. It should be noted that prior to the rapid heating, the sample was not allowed to cool to temperatures below T_a, to avoid any decomposition of the residual austenite to martensite.

In these circumstances, the reverse transformation to austenite does not require any nucleation, simply the movement of already existing ferrite–

austenite interfaces. Nevertheless, reaustenitization is not found to commence immediately the temperature is raised above T_a, even though the alloy may be in the $\alpha + \gamma$ phase field [5, 6]. This is because both acicular ferrite and bainite grow by a diffusionless displacive transformation mechanism in which the excess carbon is rejected into the austenite immediately after each growth event. This ensures that the transformation ceases prematurely, when the carbon concentration of the residual austenite (*i.e.* C^{γ}) approaches a limiting value $C^{T_0'}$ beyond which it is thermodynamically impossible for the austenite to undergo diffusionless transformation [13–17]*. After isothermal transformation to bainite (or acicular ferrite) at T_a has ceased, reaustenitization can only occur when the alloy is heated to a temperature where the carbon concentration of the residual austenite (now given by $C^{\gamma} = C^{T_0'}$) exceeds its equilibrium concentration $C^{\gamma\alpha}$ [5, 6].

An aim of the present work was to see how the *kinetics* of the reaustenitization can be reconciled with the thermodynamic model. Since this is best done using information from isothermal experiments, we begin with the results from isothermal reaustenitization experiments on Alloy H1, which is the same as the alloy used in the earlier work [5, 15].

The experiments were carried out for two starting microstructures, one consisting of a mixture of acicular ferrite and austenite, and the other of bainite and austenite (Fig. 1). Specimens of Alloy H1 were first fully austenitized (at a temperature T_1 for a time period t_1) and then quenched to a temperature $T_a = 460$ °C where they were held for 30 min to allow the formation of either acicular ferrite ($T_1 = 1200$ °C, $t_1 = 30$ min) or bainite ($T_1 = 950$ °C, $t_1 = 10$ min). Acicular ferrite has a transformation mechanism which is essentially identical to that of bainite [13, 15, 16]. Its detailed morphology differs from that of bainite because it nucleates intragranularly at inclusions within the austenite grains, whereas bainite growth begins from the austenite grain surfaces. Hence, in a steel containing suitable inclusions, a large austenite grain size favours the formation of acicular ferrite, whereas bainite growth from the austenite grain boundaries swamps the formation of acicular ferrite when the austenite grain size is relatively small. This is the reason why the change in austenitizing conditions leads to the formation of morphologically different microstructures even though the subsequent transformation conditions are identical [5, 15].

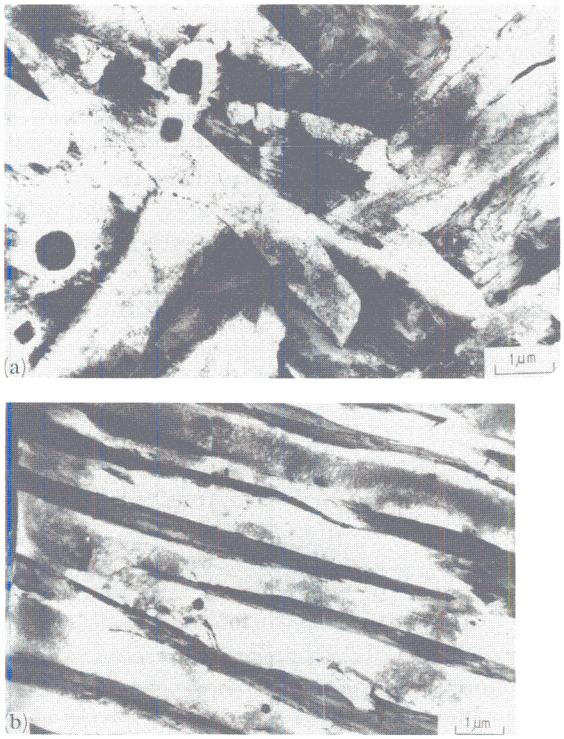

Fig. 1. Microstructures obtained after isothermal transformation of Alloy H1 at 460 °C for 30 min: (a) acicular ferrite ($T_1 = 1200$ °C, $t_1 = 30$ min); (b) bainite ($T_1 = 950$ °C, $t_1 = 10$ min).

It is important to note that the holding time of 30 min at $T_a = 460$ °C is long enough to allow the acicular ferrite or bainitic transformation to stop [5, 6, 15]. Furthermore, cementite precipitation does not accompany the formation of bainite or acicular ferrite during the isothermal heat treatment of Alloy H1 [15]; this means that the formation of cementite does not mingle with the growth of the ferrite, and that the carbon concentration of the residual austenite can be calculated using a simple mass balance procedure [18]. The mean carbon concentration of the austenite at the point where the reaction stops is

*It is experimentally established that austenite cannot transform to bainite or acicular ferrite if its carbon concentration at any transformation temperature exceeds that given by the T_0' curve on the phase diagram [13–16]. This curve is the locus of all conditions for which austenite and ferrite (with a stored energy of about 400 J mol^{-1} [14–16]) of the same composition have equal free energies. Both bainite and acicular ferrite seem to grow by diffusionless transformation, but because of the relatively high temperatures at which they form, any excess of carbon in the ferrite is rejected into the austenite immediately after transformation. The stored energy term is largely due to the invariant-plane strain shape change accompanying transformation.

given by the T_0' curve of the phase diagram (Fig. 2). After 30 min at T_a, the samples were (without cooling below T_a) rapidly heated to a higher temperature T_γ for isothermal reaustenitization.

The results are presented in Fig. 3. Since both the driving force for reaustenitization and the diffusion coefficient increases with temperature, the rate of reaction increases indefinitely with T_γ. For this reason, the experiments are restricted to fairly low reaustenitization temperatures to avoid transformation during heating. In previous work on Alloy H1 [5, 15], where it was the maximum degree of reaustenitization which was of primary interest rather than the rate of reaction, it was found that for $T_\gamma > 735$ °C, it was not possible to avoid some transformation during heating to T_γ. As will be evident later, the theory for austenite growth as presented here is subject to a number of important approximations, which are not severe for the early stages of reaustenitization. The experimental data presented in Fig. 3 therefore emphasize relatively short time periods, during which the reactions do not proceed to their maximum extents. Longer term heat treatments have been reported elsewhere for acicular ferrite and bainite of Alloy H1. Figure 4 shows a comparison of published data [5, 15] on the maximum extent of austenite obtained as a function of T_γ and the initial microstructure. It is evident that there is no significant difference between the bainite and acicular ferrite starting microstructures, and indeed, none is expected since the limiting austenite volume fraction should be determined by alloy chemistry alone.

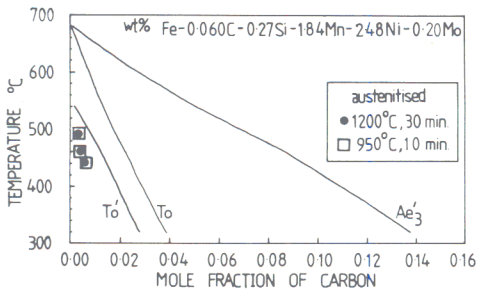

Fig. 2. Calculated phase diagram for Alloy H1 [5, 15]. The calculations are carried out using the method detailed in ref. 14. The T_0 curve is the locus of points where the austenite and ferrite of the same composition have equal free energies. The T_0' curve is similar, but allows for 400 J mol^{-1} of stored energy in the ferrite, owing to the invariant-plane strain shape change accompanying transformation. The Ae_3' curve represents the $(\alpha+\gamma)$-γ paraequilibrium phase boundary. Paraequilibrium between austenite and ferrite implies that the two phases have a substitutional solute-to-iron atom ratio which is identical everywhere, but subject to that constraint, the carbon redistributes and achieves equality of chemical potential in all phases. The points plotted represent the carbon concentrations of the residual austenite when the growth of α_b or α_a stops [5, 15].

However, the rates of transformation at any stage during the growth of austenite are found to differ significantly depending on whether the initial microstructure contains acicular ferrite or bainite (Fig. 3). The transformation rate to austenite is always found to be slower for acicular ferrite when compared with bainite. The difference in rates becomes smaller as the isothermal reaustenitization temperature increases, since the transformation rates also increase.

The time periods taken for the initiation of transformation, *i.e.* to reach a detectable degree of reaustenitization, are tabulated in Table 2 for a variety of heat treatments. The corresponding TTT curves are shown in Fig. 5; the curves do not adopt the classical C shape since for the present circumstances, both the driving force for transformation and the diffusion coefficients increase with transformation temperature, so that the overall rate of reaction must increase monotonically with temperature.

The TTT curves for the initiation of transformation might be considered subjective since it is difficult to resolve the very beginning of transformation. To calculate the TTT curves corresponding to an increase of 0.05 in the volume fraction of austenite, it is necessary to convert the length changes detected into changes in volume fraction.

An increase in the volume fraction of austenite by 0.05, during isothermal transformation, can be expressed in terms of the relative length change $\Delta L/L$ detected dilatometrically as

$$\frac{\Delta L}{L} = \frac{1}{3}\,\frac{a_{\gamma F}^{\,3} + 2a_{\alpha F}^{\,3}(1-V_{\gamma F}) - a_{\gamma I}^{\,3}V_{\gamma I}^{\,3} - 2a_{\alpha I}^{\,3}(1-V_{\gamma I})}{a_{\gamma I}^{\,3}V_{\gamma I}^{\,3} - 2a_{\alpha I}^{\,3}(1-V_{\gamma I})} \qquad (1)$$

where $a_{\gamma F}$ is the lattice parameter of austenite after a specified amount of isothermal reaustenitization (in this case an increase in the volume fraction of austenite by 0.05); $a_{\gamma I}$ is the lattice parameter of austenite at the beginning of isothermal reaustenitization; $V_{\gamma F}$ is the volume fraction of austenite after a specified amount of isothermal reaustenitization; $V_{\gamma I}$ is the volume fraction of austenite at the beginning of isothermal reaustenitization; $a_{\alpha F}$ is the lattice parameter of

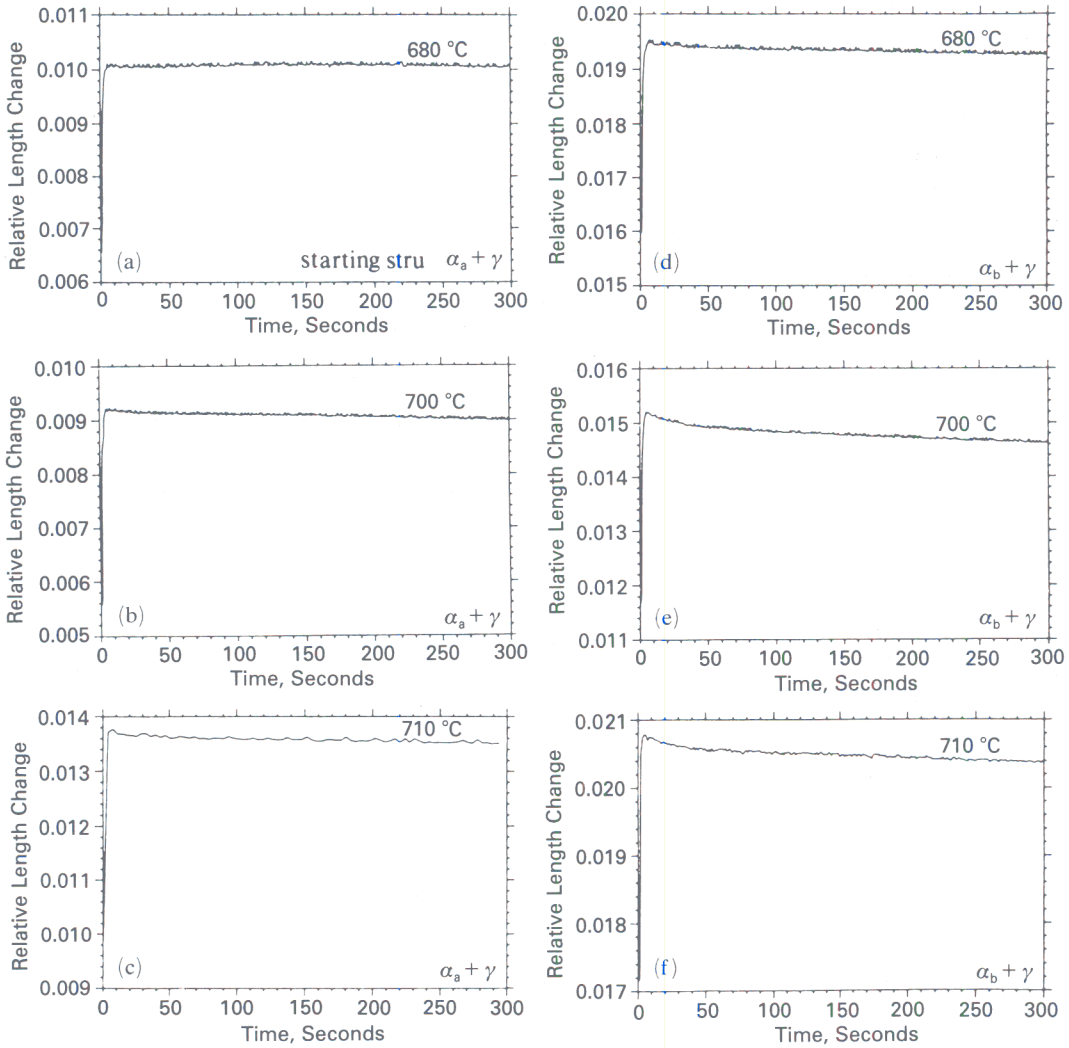

Fig. 3. Examples of dilatometric data from isothermal reaustenitization experiments, for the early stages of transformation.

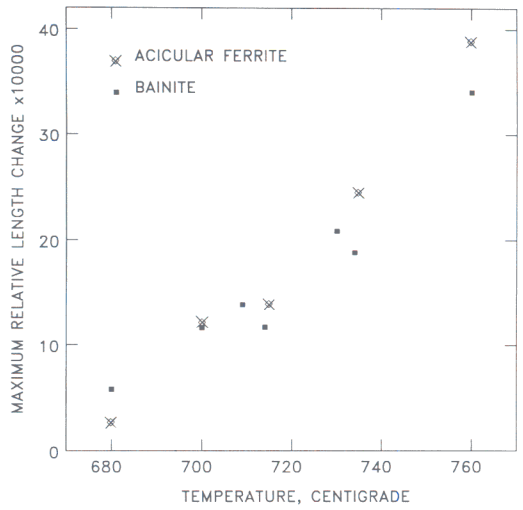

Fig. 4. Plot of the maximum relative length decrease (*i.e.* a measure of the maximum volume fraction of austenite) obtained during isothermal reaustenitization as a function of the transformation temperature T_γ. The results from two different starting microstructures ($\alpha_b+\gamma$ and $\alpha_a+\gamma$) are illustrated. Data from Yang and Bhadeshia [5, 15].

ferrite after a certain specified amount of reaustenitization; $a_{\alpha I}$ is the lattice parameter of ferrite at the beginning of reaustenitization.

The lattice parameter of the ferrite in Alloy H1 has been measured [15] using a Debye–Scherrer technique to be 0.28723 nm at ambient temperature; that of austenite is calculated as in ref. 18. To calculate these parameters at the relevant transformation temperatures, the expansion coefficients of austenite and ferrite have been

TABLE 2 The time taken for detectable reaustenitization when the initial microstructure is either $\alpha_a + \gamma$ or $\alpha_b + \gamma$

Temperature (°C)	$\alpha_a + \gamma$ *Time* (s)	$\alpha_b + \gamma$ *Time* (s)
680	250	30
690	90	15
700	30	6
710	10	4
720	5	3

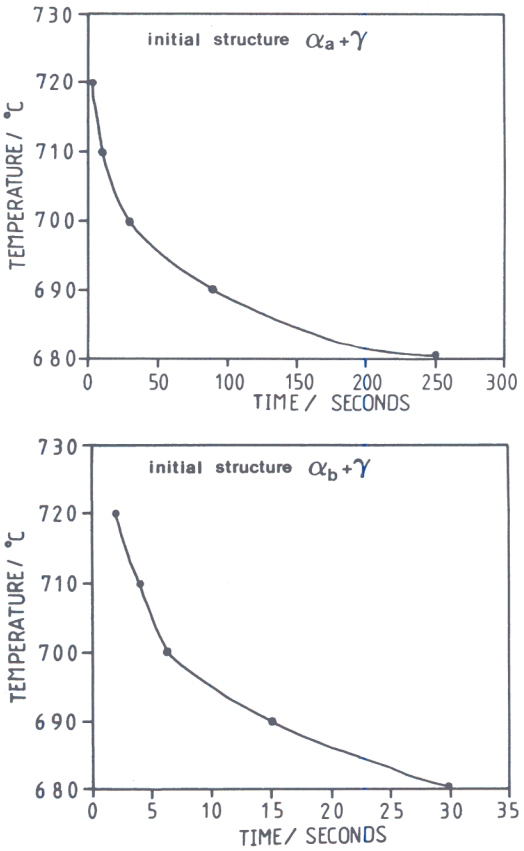

Fig. 5. TTT curves for a detectable quantity of reaustenitization: (a) initial microstructure of $\alpha_a + \gamma$; (b) initial microstructure of $\alpha_b + \gamma$.

measured [15] to be 1.769×10^{-5} K^{-1} and 1.15×10^{-5} K^{-1} respectively.

Since for the present work, the specified increment in the volume fraction of austenite is taken to be 0.05, we have

$$V_{\gamma F} = 0.05 + V_{\gamma I} \tag{2}$$

If the resulting small change in the carbon concentration of the austenite is ignored, then

$$a_{\gamma F} \simeq a_{\gamma I} \tag{3}$$

and

$$a_{\alpha F} \simeq a_{\alpha I} \tag{4}$$

The equation for length change as a function of the change in volume fraction of austenite thus simplifies to

$$\frac{\Delta L}{L} = \frac{1}{3} \frac{0.05 a_{\gamma I}^{\ 3} - 0.1 a_{\alpha I}^{\ 3}}{V_{\gamma I} a_{\gamma I}^{\ 3} + 2(1 - V_{\gamma I}) a_{\alpha I}^{\ 3}} \tag{5}$$

The above equations were used to derive the data presented in Table 3, and the 5% transformation TTT curves plotted in Fig. 6. The general trends are confirmed to be identical to the results

TABLE 3 The time taken for increasing the volume fraction of γ by 0.05 when the initial microstructure is either $\alpha_a + \gamma$ or $\alpha_b + \gamma$

Temperature (°C)	$\alpha_a + \gamma$ *Time* (s)	$\alpha_b + \gamma$ *Time* (s)
680	548	300
690	370	150
700	192	110
710	114	70
720	43	26

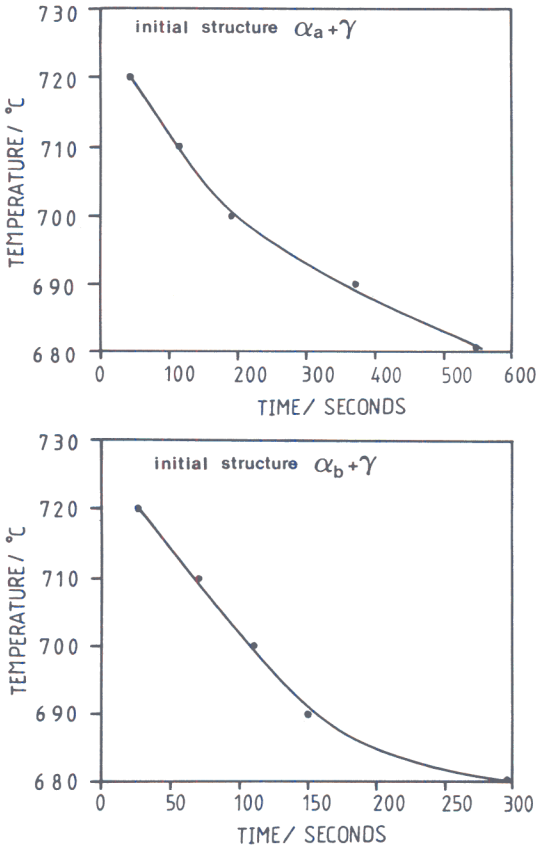

Fig. 6. TTT curves for a 0.05 increase in the volume fraction of austenite: (a) initial microstructure of $\alpha_a + \gamma$; (b) initial microstructure of $\alpha_b + \gamma$.

for the initiation of transformation (Table 2, Fig. 5).

3.2. Kinetic theory

To further interpret the results of the isothermal reaustenitization experiments, it is necessary to identify the main factors influencing the rate of austenite growth, as a function of alloy chemistry, temperature and the two starting microstructures pertinent to the present study. The problem is simplified by the fact that austenite nucleation need not be considered since the experiments are designed to reflect just its growth.

Since both bainite and acicular ferrite are in the form of thin plates, the movement of the planar austenite–ferrite interfaces can during the early stages of reverse transformation be modelled in terms of one-dimensional growth. For simplicity, it is assumed that growth is diffusion-controlled. All the redistribution of carbon must occur within the austenite during its growth, since the amount of carbon in the ferrite is negligible. Microanalysis experiments have demonstrated that the reaustenitization process involves the diffusional growth of austenite in Alloy H1 for the conditions used in the present study, with substitutional elements partitioning between the austenite and ferrite [5, 15]. The extent of substitutional solute partitioning is known to decrease with an increase in driving force (which in turn increases with T_γ). The microanalysis experiments are not of sufficient spatial resolution to identify the compositions at the transformation interface, but it is likely that local equilibrium exists at the interface for low T_γ with a tendency towards zero bulk partitioning (*i.e.* negligible-partitioning local equilibrium or paraequilibrium [19–27] as T_γ increases to beyond the Ae_3 temperature of the alloy. This makes a full analysis impossible since it is not yet possible to determine theoretically, which of these infinite possibilities, between the limits of local equilibrium and paraequilibrium, that the system chooses to adopt as a function of temperature. In other words, the compositions of the phases at the interface cannot as yet be deduced theoretically.

If local equilibrium is achieved at least approximately at the transformation interface, then the growth rate calculated assuming carbon diffusion-controlled motion of the γ–α interface, using the *equilibrium* carbon concentrations may give a good guide to the factors influencing the kinetics of transformation. This amounts to assuming that the effect of substitutional solute gradients in influencing the flux of carbon is zero [20, 23]. There is a further implicit assumption that the tie-line (of the equilibrium phase diagram) which determines the interface compositions passes through the bulk composition of the alloy. This is unlikely in substitutionally alloyed steels [19–22], but may be a good approximation since the alloys considered here are dilute.

Finally, any effects owing to soft impingement (overlap of diffusion fields) are not taken into account, since it is only the early stages of transformation that are considered in the present study. Hence, the austenite and ferrite are both in effect assumed to be semi-infinite in extent.

One-dimensional diffusion-controlled growth involves the parabolic thickening of layers of austenite. The increase in the half-thickness of austenite can therefore be described as [23, 28]

$$q = \alpha_1 t^{1/2} \tag{6}$$

$$\mathrm{d}q = 0.5\alpha_1 t^{-1/2}\mathrm{d}t \tag{7}$$

where q is the *increase* in the half-thickness of the austenite layer, of starting thickness a_0, and α_1 is the one-dimensional parabolic thickening rate constant.

The geometry assumed for the thickening of austenite layers is based on the plate shape of bainite or acicular ferrite. If c is the largest dimension of a bainitic ferrite plate, idealized as a rectangular parallelepiped with sides of length a, b and c, with $c = b \gg a$, then when both of the sides of a ferrite plate are penetrated by the growing austenite, the total area of the γ–α interface which advances into the plate of ferrite is $2c^2$. This reduces the thickness of the plate by $\Delta a_\mathrm{m}/2$ from either side. If the minimum detectable change in volume fraction is ΔV_v, then it follows that

$$\Delta V_\mathrm{v} = 2N_\mathrm{v}c^2 \int_0^{\Delta a_\mathrm{m}/2} \mathrm{d}q \tag{8}$$

where N_v is the initial number of particles of austenite per unit volume, and Δa_m is the minimum detectable thickness increase.

On combining eqns. (7) and (8), we get

$$\Delta V_\mathrm{v} = 2N_\mathrm{v}c^2 \int_0^{\tau} 0.5\alpha_1 t^{-1/2}\mathrm{d}t \tag{9}$$

where τ is the time taken for the minimum detectable transformation. After integration, this

becomes

$$\Delta V_v = 2\alpha_1 N_v c^2 \tau^{1/2} \tag{10}$$

so that

$$\tau = \left(\frac{\Delta V_v}{2\alpha_1 N_v c^2}\right)^2 \tag{11}$$

However,

$$2N_v c^2 = S_v = 2/\bar{L}$$

so that

$$\tau = \left(\frac{\Delta V_v}{\alpha_1 S_v}\right)^2 \tag{12}$$

where S_v is the surface area of $\gamma-\alpha$ boundary per unit volume, and $1/\bar{L}$ is the number of intercepts of $\gamma-\alpha$ boundary per unit length of test line [29]. It is clear from eqn. (12), that the value of τ is dependent on not only the parabolic rate constant α_1 but also the surface area of the $\gamma-\alpha$ interface per unit volume S_v for a specific amount of reaustenitization.

For the same starting microstructure and a specific amount of transformation, τ decreases rapidly as the isothermal reaustenitization temperature increases due to the increase in α_1. Equation (12) also indicates that the morphology of the starting microstructure will effect τ, because S_v must depend on the detailed nature of the initial microstructure. As will be seen later, this could explain the different rates at which the $\alpha_b + \gamma$ and $\alpha_a + \gamma$ reaustenitize. The analysis shows that for a specified amount of reaustenitization, and a fixed initial microstructure

$$\tau \propto \frac{1}{\alpha_1^2} \tag{13}$$

3.3. Estimation of the parabolic thickening rate constant

The parabolic rate constant α_1 can be deduced by analogy with already existing theory for the $\gamma \rightarrow \alpha$ transformation [23, 30–32]. Figure 7 shows the carbon concentration profiles in α and γ before reaustenitization and during austenite growth; the austenite must become more dilute in carbon as it grows, the rate of interface motion being determined by the diffusion of carbon in the austenite behind the interface. In Fig. 7(a), C^1 is the carbon concentration in the austenite before the start of reaustenitization; it is given by

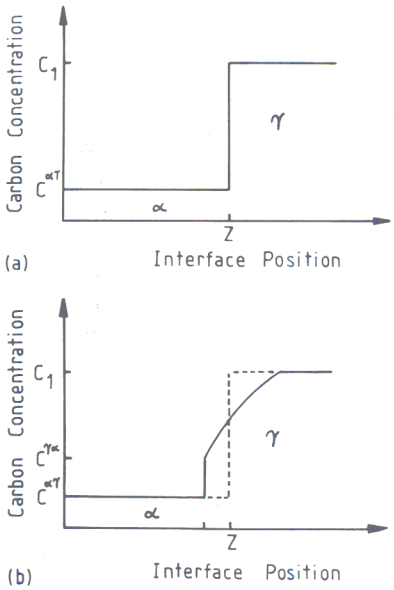

Fig. 7. The distribution of carbon, (a) before reaustenitization, and (b) during reaustenitization. C^1 is the carbon concentration in austenite, $C^{\gamma\alpha}$ is the carbon concentration in austenite at the $\gamma-\alpha$ interface during reaustenitization, and $C^{\alpha\gamma}$ is the carbon concentration in α at the $\alpha-\gamma$ interface during reaustenitization.

$C^1 = C^{T'_0}$; for $T_a = 460$ °C, $C^{T'_0} = 0.01235$ mole fraction of carbon (Fig. 2). In Fig. 7(b), the carbon concentration of γ at the $\gamma-\alpha$ interface during reaustenitization is $C^{\gamma\alpha}$, and the carbon concentration of γ far away from the interface remains C^1. It is assumed that the carbon concentration of α remains the same, $C^{\alpha\gamma}$, before and during reaustenitization. The coordinate z is defined normal to the $\gamma-\alpha$ interface.

During reaustenitization the flux of carbon in the austenite, towards the $\gamma-\alpha$ interface, at the position of interface can be expressed as

$$J = -D\{C^{\gamma\alpha}\}\left(\frac{\partial C}{\partial Z}\right) \tag{14}$$

where the use of braces implies a functional relationship, *i.e.* $D\{C^{\gamma\alpha}\}$ implies that the function D is evaluated at the concentration $C^{\gamma\alpha}$. The diffusion coefficient of carbon in austenite D is known to be strongly concentration dependent [33–37]. We assume that a weighted average diffusivity $\bar{D}$ can adequately represent the effective diffusivity of carbon [38] in the concentration gradient; it is given by

$$\bar{D} = \int_{C^1}^{C^{\gamma\alpha}} D\,\mathrm{d}C/(C^{\gamma\alpha} - C^1) \tag{15}$$

The rate at which carbon concentration of austenite is diluted can be written as

$$R = v(C^1 - C^{\alpha\gamma}) \tag{16}$$

where v is the velocity of interface.

Given that the position Z of the interface along the coordinate z is defined by the equation

$$Z = \alpha_1 t^{1/2}$$

it follows that

$$v = \frac{dZ}{dt} = 0.5\alpha_1 t^{-1/2} \tag{17}$$

Combining eqns. (16) and (17), the rate at which carbon concentration of γ is diluted can be expressed as

$$R = 0.5\alpha_1 t^{-1/2}(C^1 - C^{\alpha\gamma}) \tag{18}$$

Conservation of mass at the interface requires that (*i.e.* combining eqns. (14) and (18))

$$0.5\alpha_1 t^{-1/2}(C^1 - C^{\alpha\gamma}) = -\bar{D}\left(\frac{\partial C}{\partial Z}\right)_{z=Z} \tag{19}$$

where z is the coordinate normal to the interface plane and Z is the position of the interface along the coordinate z. The concentration gradient $\partial C/\partial Z$ in eqn. (19) is evaluated at the position of the interface, *i.e.* at $z = Z$. Equation (19) simply states that the rate of dilution of the austenite, per unit of time, equals the carbon flux towards the γ–α interface. From Fick's laws, the differential equation for the matrix is given by

$$\frac{\partial C}{\partial t} = \frac{\partial\{\bar{D}(\partial C/\partial Z)\}}{\partial Z} \tag{20}$$

subject to the boundary condition $C = C^{\gamma\alpha}$ at $z = Z\{t\}$, and $C = C^1$ at $t = 0$, and eqn. (19). It can be solved [23, 30–32] to give an implicit relation for α_1 as a solution of the form

$$f_1 = \frac{C^1 - C^{\gamma\alpha}}{C^1 - C^{\alpha\gamma}} = H_1\{\bar{D}\} \tag{21}$$

where

$$H_1\{\bar{D}\} = \left(\frac{0.25\pi}{\bar{D}}\right)^{0.5} \alpha_1 \left[\operatorname{erfc}\left\{\frac{0.5\alpha_1}{\bar{D}^{0.5}}\right\}\right] \exp\left\{\frac{\alpha_1^2}{4\bar{D}}\right\} \tag{22}$$

Finally the parabolic rate constant α_1 can be calculated using eqns. (21) and (22) with the diffusivity calculated as in ref. 37.

3.4. The relationship between the parabolic rate constant and TTT curves

Values of the parabolic thickening rate constants for reaustenitization, calculated using the above procedures are given in Table 4.

Consistent with the theory discussed earlier, Figs. 8 and 9 show that τ is found experimentally to be proportional to $1/\alpha_1^2$, the linear correlation coefficients in all cases being extremely good.

It was earlier shown that the rate of reaustenitization tends to be larger when the starting microstructure is bainite rather than acicular ferrite. Acicular ferrite plates, because they nucleate intragranularly from "point" nucleation sites, are usually found in non-parallel formations well dispersed in the austenite, whereas bainite tends to form in sheaves consisting of parallel platelets. It is therefore intuitively expected that the amount of γ–α interface per unit volume of sample (S_v) should be different for the two microstructures. This would obviously have an effect on reaustenitization kinetics. For these two different starting microstructures, the mean number of intercepts $1/\bar{L}$ of γ–α boundary per unit length of test line in were in each case measured on transmission electron micrographs (using 50 test lines at random transmission electron micrographs magnified 10 000×). The results are $1/\bar{L} = 0.78 \pm 0.15$ μm^{-1} for $\alpha_a + \gamma$, and $1/\bar{L} = 1.07 \pm 0.12$ μm^{-1} for $\alpha_b + \gamma$. The corresponding values for the γ–α interface area per unit volume are $S_v = 1.56 \pm 0.30$ μm^{-1} for $\alpha_a + \gamma$, and $S_v = 2.14 \pm 0.24$ μm^{-1} for $\alpha_b + \gamma$.

For a specified extent of transformation to austenite, eqn. (12) indicates that

$$\tau \propto \frac{1}{(S_v\alpha_1)^2} \tag{23}$$

TABLE 4 The parabolic constant α_1 at different reaustenitization temperatures

Temperature (°C)	α_1 (cm $s^{-0.5}$)	$1/\alpha_1^2$ (s cm^{-2})
680	0.9968×10^{-5}	0.1006×10^{11}
690	0.2017×10^{-4}	0.2459×10^{10}
700	0.3350×10^{-4}	0.8911×10^{9}
710	0.5679×10^{-4}	0.3101×10^{9}
720	0.8300×10^{-4}	0.1452×10^{9}

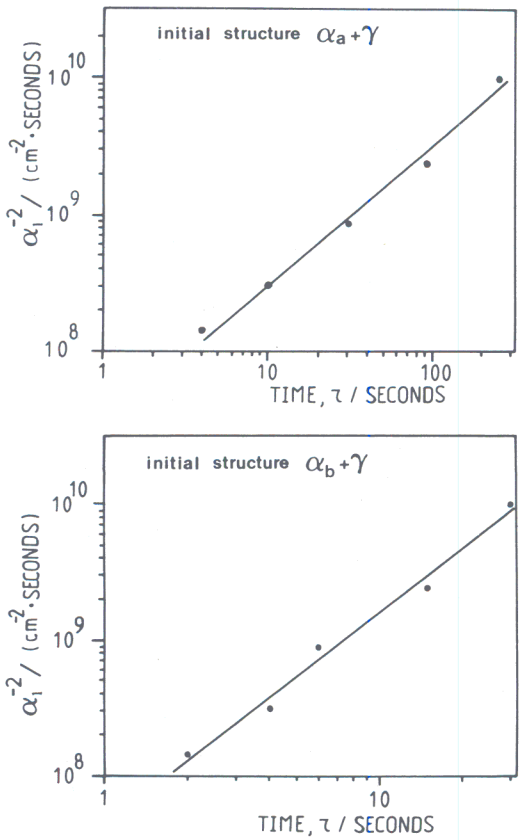

Fig. 8. Linear relationship between the time τ taken for a detectable amount of transformation and the quantity $1/\alpha_1^2$: (a) initial microstructure $\alpha_a+\gamma$; (b) initial microstructure of $\alpha_b+\gamma$.

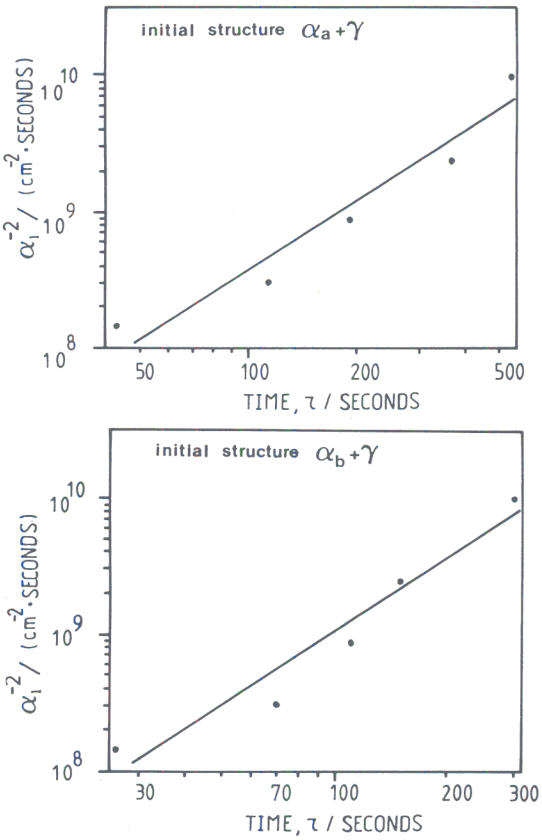

Fig. 9. Linear relationship between the time τ taken for an increase in the volume fraction of austenite by 0.05, and $1/\alpha_1^2$: (a) initial microstructure $\alpha_a+\gamma$; (b) initial microstructure $\alpha_b+\gamma$.

It is clear that the amount of γ–α grain boundary area per unit volume is an important factor in explaining why τ is larger in the case of $\alpha_a+\gamma$.

3.5. Continuous heating transformation

Although large deposition rates can sometimes be used to fabricate single pass welds between thick plates, the associated high heat input is detrimental to mechanical properties. Critical applications therefore involve the filling of joints with many smaller layers of weld metal, each layer deposited in a sequence designed to optimize the weld quality. In such multirun welds, all the layers other than the final one, experience heating and cooling cycles after the melt has cooled to the interpass temperature, as a consequence of the heat input as successive layers are deposited. In terms of the influence on microstructure, the thermal cycle experienced as an adjacent layer is deposited is expected to be most important, since it will be associated with the highest peak temperature. It is appropriate therefore to begin a study of anisothermal reaustenitization, with an initial microstructure which is the primary weld microstructure, *i.e.* the microstructure which evolves during the cooling of the weld from the liquid state. A multirun weld will, of course, contain a whole range of complex microstructures since many regions of the weld can have experienced a whole series of thermal cycles by the time the joint is filled. The problem of reaustenitization in multirun welds is therefore more complex than has been possible to investigate in this work, which focuses on the reaustenitization of the microstructure of the last bead to be deposited.

This microstructure has been verified to consist of a mixture of acicular ferrite and microphases (*i.e.* martensite and retained austenite); carbides are absent and allotriomorphic ferrite is found in extremely small quantities (less than 5%) in regions where the alloy content is lowered by chemical segregation.

High speed dilatometry was used to study and

compare the CHT behaviour of the as-deposited regions of three different welds (Alloys 1, 2 and 3). The dilatometer specimens were heated from ambient temperature to 950 °C at a variety of heating rates ranging from 0.06 → 56 °C s^{-1}. Figure 10 shows plots of the relative length change owing to thermal expansion and transformation as a function of time (which is directly proportional to temperature during heating, since the heating rates used were constant). Transformation start temperatures were measured from these data, as illustrated in Fig. 11.

Decomposition of austenite during heating was not observed in any of the samples during heating to temperatures as high as 600 °C, even at the slowest heating rate used (0.06 °C s^{-1}). This is evident from the constant slopes of the curves shown in Fig. 10.

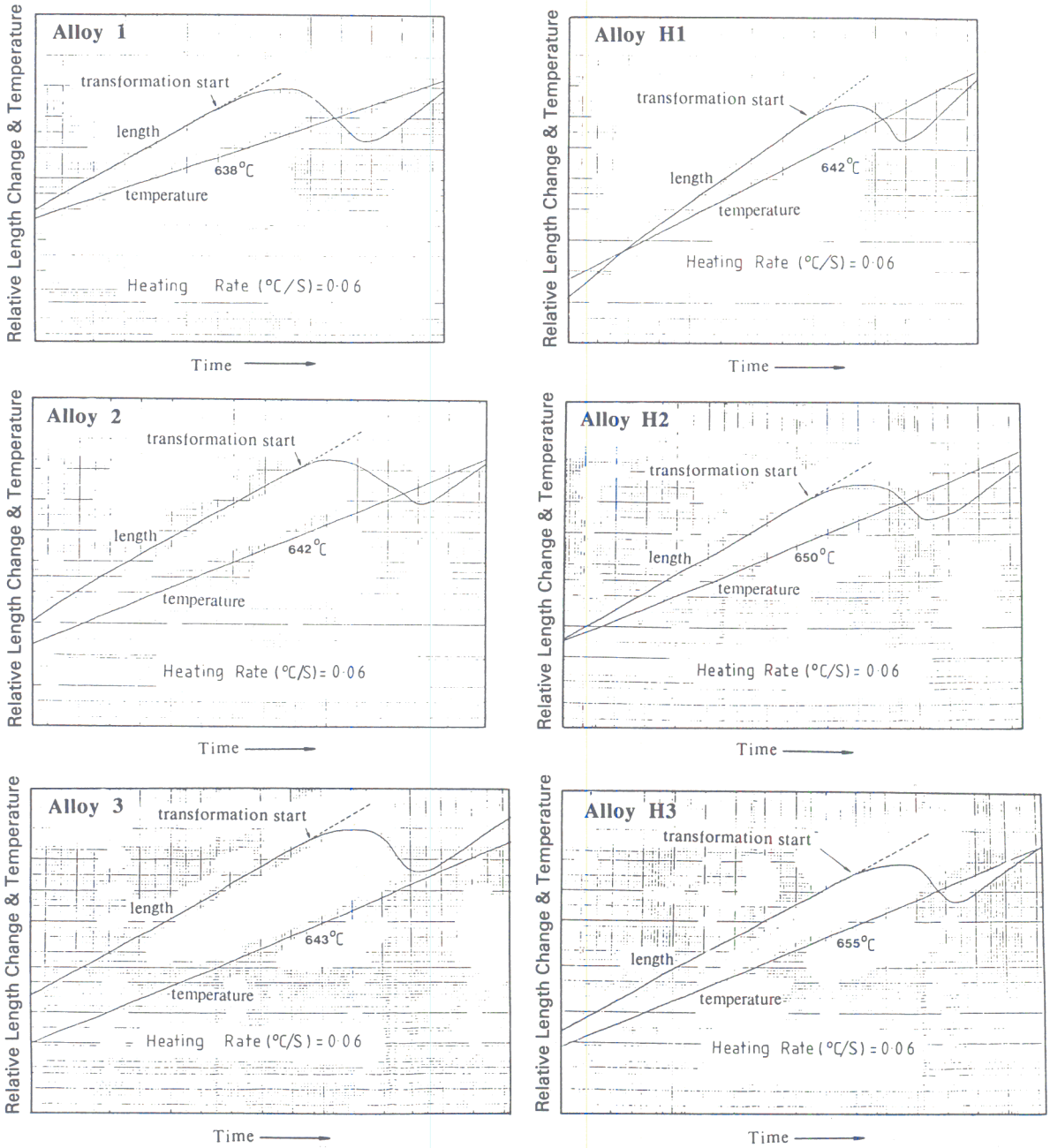

Fig. 10. Examples of dilatometric data from continuous heating experiments on Alloys 1, 2 and 3.

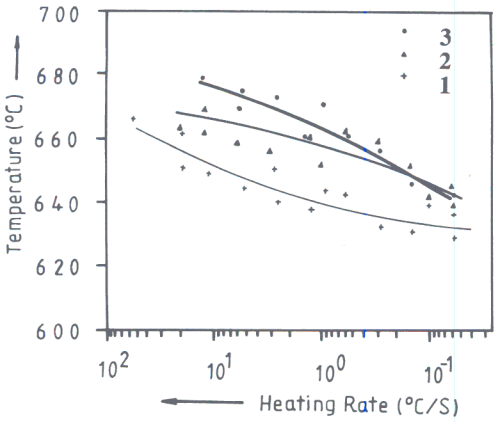

Fig. 11. Transformation start temperatures from continuous heating experiments, for Alloys 1, 2 and 3.

The behaviour during continuous heating should be related to the isothermal transformation kinetics. For example, the continuous heating curve could be treated as a series of small isothermal steps, each occurring at a successively higher temperature, with a time interval t_i associated with each step (where i is the subscript identifying the step number). If the time necessary to reach a specified increment of transformation is written as τ_i for the isothermal transformation temperature T_i, then the simplest approximation is to assume Scheil's rule [28]. In this, the specified increment of transformation is achieved during continuous heating when the sum

$$\sum_{i=1}^{n} \frac{t_i}{\tau_i} = 1 \qquad (24)$$

An application of this rule to the τ values listed in Table 2, for the $\alpha_a + \gamma$ starting microstructure, showed that during continuous heating (0.06 °C s^{-1}) of that microstructure, reaustenitization should begin at a temperature of about 685 °C. It is, however, evident from Fig. 11 that for the same heating rate, the as-deposited welds begin to transform to austenite at a much lower temperature of about 630 °C.

Of course, the incubation time data of Table 2 refer to reaustenitization from an initial microstructure generated by isothermal transformation to acicular ferrite or bainite at 460 °C. However, the primary weld microstructure arises during continuous cooling of the weld to ambient temperature. The carbon concentration C_γ of the austenite in the weld may then be approximated by $C^{T'_0}$ evaluated at the martensite-start M_s temperature of the alloy concerned. This is because the weld can be assumed to continue transforming to acicular ferrite until the M_s temperature is reached. Unfortunately, the composition of the residual austenite is expected to change as acicular ferrite forms, so that its M_s temperature is not easy to evaluate, especially if the carbon is inhomogeneously distributed in the austenite [39–41]. Nonetheless, the values of $C^{T'_0}$ evaluated at the M_s temperature of the untransformed alloy must provide a lower limit to the carbon concentration of the residual austenite. Since this is larger than the corresponding value at 460 °C, it is not surprising that the welds begin the reaustenitization process at lower temperatures and at faster rates when compared with isothermal reaustenitization in which the initial microstructure was generated by transformation at 460 °C.

In fact, the rate at which the reaustenitization start temperature T_γ^s is expected to decrease as the temperature T_a for the isothermal formation of acicular ferrite decreases, is given by

$$\frac{\partial T_\gamma^s}{\partial T_a} = \frac{S_{T'_0}}{S_{Ae_3}} \qquad (25)$$

where $S_{T'_0}$ and S_{Ae_3} refer to the slopes of the T'_0 and Ae_3 curves of the phase diagram respectively. For Alloy 1, the ratio $S_{T'_0}:S_{Ae_3}$ is found to be 2.36 (Fig. 2) for the carbon concentration range 0→0.04 mole fraction on the phase diagram. Since the difference in $T_\gamma^s\{0.06\ °C\ s^{-1}\}$ between the samples isothermally transformed at 460 °C and the as-welded microstructure is 685–630 °C, the *effective value* of T_a for the as-welded microstructure is estimated to be 436 °C. Using this equation, it is evident that the effective values of T_a associated with the as-welded microstructures of Alloys 1, 2 and 3, for the slowest heating rates used (*i.e.* approaching equilibrium transformation) scale approximately with the M_s temperatures of the alloys.

The essential difference between Alloys 2 and 3 is that the former contains an additional quantity of molybdenum (about 0.2 wt.%) and hence transforms to austenite at a relatively lower temperature when the heating rate is rapid, but at a relatively higher temperature for lower heating rates. This is consistent with the calculated TTT curves (for the $\alpha \rightarrow \gamma$ reaction) illustrated in Fig. 12. The diagrams illustrate that at relatively high transformation temperatures, at least as far as the alloys used in this work are concerned, austenite is stabilized by the addition of molybdenum,

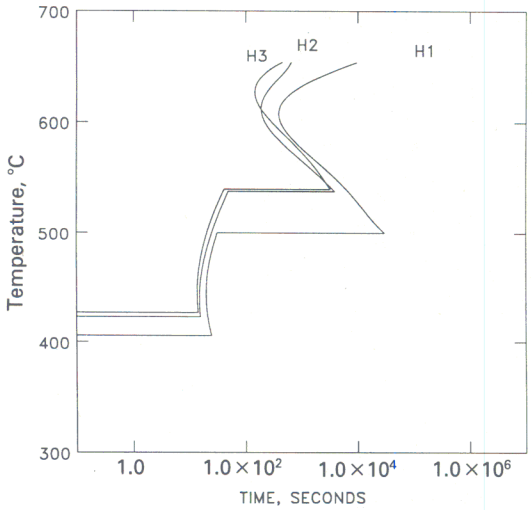

Fig. 12. Calculated TTT curves [42, 43] for Alloys H1, H2 and H3.

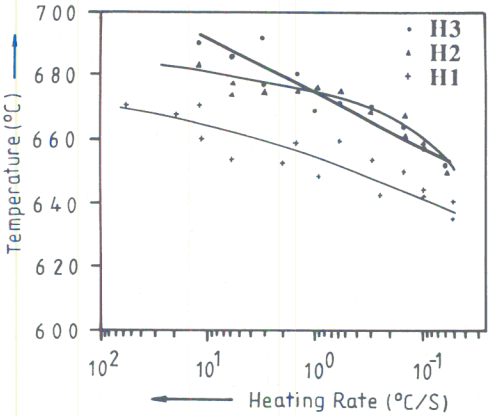

Fig. 13. Transformation start temperatures from continuous heating experiments, for Alloys H1, H2 and H3. The starting microstructures were in all cases martensitic.

whereas for transformations at relatively low temperatures, ferrite is stabilized by the addition of molybdenum. The trend was confirmed for the corresponding homogenized samples (Fig. 13), where the starting microstructure was martensite. Finally, it is expected that the transformation temperature for Alloy 1 should always be lower than of Alloys 2 and 3 because it contains a higher level of carbon, manganese and nickel, the results again being consistent with the calculated TTT diagrams presented in Fig. 12.

3.6. Transmission electron microscopy

The purpose of transmission electron microscopy was to establish some of the basic assumptions made in modelling the reaustenitization process.

The microstructures of acicular ferrite and bainite, obtained after isothermal transformation at 460 °C, are illustrated in Figs. 14(a) and 14(b). Figures 14(c)–14(e) show that the basic assumption that the reaustenitization process in these samples involves the planar advance of austenite–ferrite interfaces is essentially justified, since the films of austenite are seen to thicken.

4. Conclusions

The growth of austenite has been studied during the heating of microstructures containing bainitic ferrite and austenite, or acicular ferrite and austenite. Since the initial shape of the ferrite regions in these microstructures is that of thin plates, it has been found possible to model the early stages of austenite growth in terms of the one-dimensional carbon diffusion-controlled movement of planar austenite–ferrite interfaces. In these circumstances, the time required to achieve a specified degree of austenite growth is found to be proportional to the product $S_v^{-2}\alpha_1^{-2}$, where S_v is the amount of austenite–ferrite interface per unit volume and α_1 is the one-dimensional parabolic thickening rate constant. Although this relationship is well obeyed, there are a number of assumptions in the theoretical analysis which require further work; one such assumption requires a model capable of predicting the degree of (non-equilibrium) redistribution of substitutional solutes during transformation.

Because of the different spatial distribution of ferrite plates within the bainitic and acicular ferrite microstructures, S_v is found to be smaller for the latter, with the consequence that acicular ferrite reaustenitizes at a slower rate even though it may have been generated under identical isothermal transformation conditions.

Reaustenitization is found to commence at very low temperatures when as-deposited high-strength steel welds are subjected to continuous heating treatments. This is because the welds, after solidification, transform to acicular ferrite in such a way, that the effective temperature at which the acicular ferrite reaction is deemed to stop, is close to the overall martensite start temperature of the alloy concerned. The experiments also revealed a peculiar effect of molybdenum, which in the alloys studied, tends to stabilize

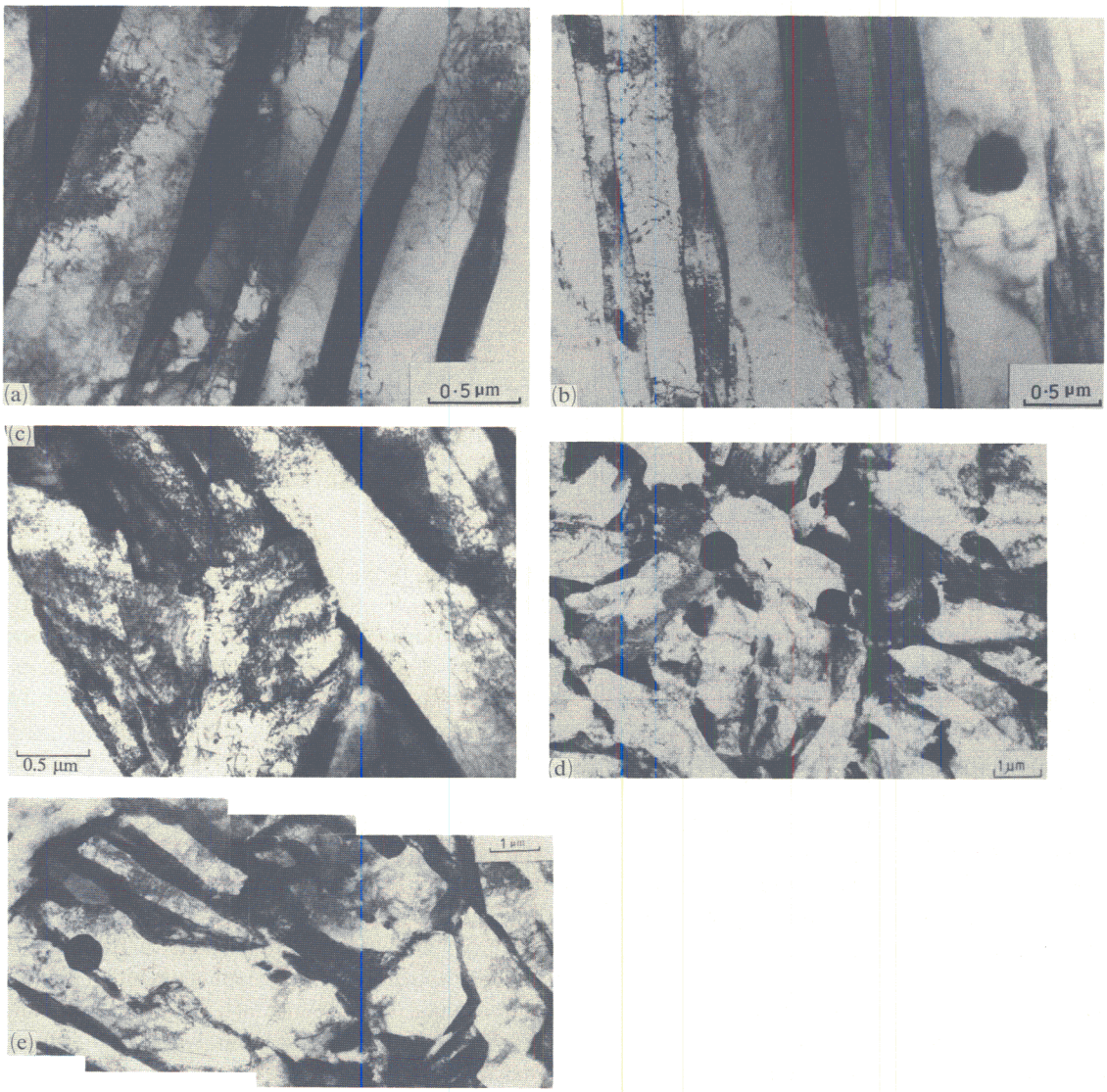

Fig. 14. Transmission electron micrographs illustrating the change in the starting microstructure owing to the growth of austenite. Since the austenite transforms to martensite on cooling, the martensite regions are to be taken as representing the austenite which existed at the reaustenitization temperature: (a) initial microstructure of bainite, after partial reaustenitization at 680 °C for 2 h; (b) initial microstructure of bainite, after partial reaustenitization at 720 °C for 2 h; (c) initial microstructure of bainite, after partial reaustenitization at 740 °C for 2 h; (d) initial microstructure of acicular ferrite, after partial reaustenitization at 680 °C for 10 min; (e) initial microstructure of acicular ferrite, after partial reaustenitization at 700 °C for 10 min.

austenite at low temperatures, but ferrite at relatively high temperatures; this behaviour is found to be consistent with the effect of molybdenum on the thermodynamics of transformation.

Acknowledgments

The authors are grateful to Professor D. Hull for the provision of laboratory facilities at the University of Cambridge, and to the Ministry of Education, Republic of China, for funding the research.

References

1 K. Tsuzaki, K. Yamaguchi, T. Maki and I. Tamura, *Tetsu to Hagane, 74* (1980) 1430–1437.
2 P. J. Alberry and W. K. C. Jones, *Met. Technol., 7* (1977) 360.
3 M. F. Ashby and K. E. Easterling, *Acta Metall., 32* (1984) 1935.
4 S. T. Kimmins and D. J. Gooch, *Met. Sci. J., 17* (1983) 519–532.
5 J. R. Yang and H. K. D. H. Bhadeshia, in J. Y. Koo (ed.), *Proc. Int. Conf. on Welding Metallurgy of Structural Steels*, The Metallurgical Society of AIME, Warrendale, PA, 1987, pp. 549–563.

6 J. R. Yang and H. K. D. H. Bhadeshia, in G. W. Lorimer (ed.), *Proc. Int. Conf. on Phase Transformations, 1987*, The Institute of Metals, London, 1988, pp. 203–206.
7 D. J. Sparkes, *Welding Inst. Res. Rep. 352/1987*, 1987 (The Welding Institute, Cambridge, U.K.).
8 N. C. Law and D. V. Edmonds, *Metall. Trans. A, 11* (1980) 33.
9 S. Matsuda and Y. Okamura, *Trans. Iron Steel Inst. Jpn., 14* (1974) 445.
10 H. K. D. H. Bhadeshia and L. E. Svensson, *J. of Mater. Sci.*, in the press.
11 L. E. Svensson and H. K. D. H. Bhadeshia, *Proc. Int. Conf. on Weld Quality and the Role of Computers*, Pergamon, Oxford, 1988, pp. 71–78.
12 R. Reed and H. K. D. H. Bhadeshia, *Int. Conf. on Trends in Welding Research*, Gatlingburg, to be presented in May, 1989.
13 H. K. D. H. Bhadeshia, in G. W. Lorimer (ed.), *Proc. Int. Conf., Phase Transformations 1987*, The Institute of Metals, London, 1988, pp. 309–314.
14 H. K. D. H. Bhadeshia and D. V. Edmonds, *Acta Metall., 28* (1980) 1265–1273.
15 J. R. Yang and H. K. D. H. Bhadeshia, in S. A. David (ed.), *Advances in the Science and Technology of Welding*, American Society for Metals, Metals Park, OH, 1987, pp. 187–191.
16 M. Strangwood and H. K. D. H. Bhadeshia, in S. A. David (ed.), *Advances in the Science and Technology of Welding*, ASM, Metals Park, OH, 1987, pp. 209–213.
17 J. W. Christian and D. V. Edmonds, in A. R. Marder and J. I. Goldstein (eds.), *Phase Transformations in Ferrous Alloys*, The Metallurgical Society of AIME, Warrendale, PA, 1984, pp. 293–326.
18 H. K. D. H. Bhadeshia, in H. I. Aaronson *et al.* (eds.), *Proc. Int. Conf. on Solid→Solid Phase Transformations*, The Metallurgical Society of AIME, Warrendale, PA, 1981, pp. 1041–1048.
19 M. Hillert, *Int. Rep., 1953* (Swedish Institute of Metals Research).
20 J. S. Kirkaldy, *Can. J. Phys., 36* (1958) 907.
21 G. R. Purdy, D. H. Weichert and J. S. Kirkaldy, *Trans. Metall. Soc. AIME, 230* (1964) 1025.
22 D. E. Coates, *Metall. Trans., 4* (1973) 2313.
23 H. K. D. H. Bhadeshia, *Prog. Mater. Sci., 29* (1985) 321–386.
24 A. Hultgren, *Jernkontorets Ann., 135* (1951) 403.
25 M. Hillert, *Jernkontorets Ann., 136* (1952) 25.
26 E. Rudberg, *Jernkontorets Ann., 136* (1952) 91.
27 H. I. Aaronson, H. A. Domian and G. M. Pound, *Trans. Metall. Soc. AIME, 236* (1966) 768.
28 J. W. Christian, *Theory of Transformations in Metals and Alloys*, Pergamon, Oxford, 2nd Edn., Part I, 1975.
29 R. T. DeHoff and F. N. Rhines (eds.), *Quantitative Microscopy*, McGraw-Hill, New York, 1968.
30 C. Zener, *J. Appl. Phys., 20* (1949) 950.
31 C. A. Dubé, *Ph.D. Thesis*, Carnegie Institute of Technology, 1948.
32 C. Atkinson, *Acta Metall., 15* (1967) 1207.
33 R. P. Smith, *J. Am. Chem. Soc., 68* (1946) 1163.
34 C. Wells, W. Batz and R. F. Mehl, *Trans. Metall. Soc. AIME, 188* (1950) 533.
35 R. H. Siller and R. B. McLellan, *Trans. Metall. Soc. AIME, 245* (1969) 697.
36 R. H. Siller and R. B. McLellan, *Metall. Trans., 1* (1970) 985.
37 H. K. D. H. Bhadeshia, *Met. Sci. J., 15* (1981) 477–479.
38 R. Trivedi and G. M. Pound, *J. Appl. Phys., 38* (1967) 3569.
39 H. K. D. H. Bhadeshia and A. R. Waugh, *Acta Metall., 30* (1982) 775–784.
40 A. Schrader and F. Wever, *Arch Eisenhuttenwes., 23* (1952) 489.
41 S. J. Matas and R. F. Hehemann, *Trans. Metall. Soc. AIME, 221* (1961) 179.
42 H. K. D. H. Bhadeshia, *Met. Sci. J., 16* (1982) 159–165.
43 H. K. D. H. Bhadeshia, *Scr. Metall., 22* (1988) I–IV.

Appendix A: nomenclature

$a_{\alpha F}$	lattice parameter of ferrite at any stage of reaustenitization
$a_{\alpha I}$	lattice parameter of ferrite at the beginning of reaustenitization
$\alpha_{\gamma F}$	lattice parameter of austenite at any stage of reaustenitization
$a_{\gamma I}$	lattice parameter of austenite at the beginning of reaustenitization
Δa_m	minimum detectable increase in austenite thickness
Ae_3	boundary separating the γ and $\alpha + \gamma$ phase fields
B_s	bainite-start temperature
c	initial length of ferrite plate
C^1	carbon concentration in the austenite before the start of reaustenitization
$C^{T_0'}$	carbon concentration given by the T_0 curve
C^γ	carbon concentration of residual austenite
$C^{\alpha\gamma}$	carbon concentration in ferrite which is in equilibrium with austenite
$C^{\gamma\alpha}$	carbon concentration in austenite which is in equilibrium with ferrite
CHT	continuous-heating transformation
D	diffusivity of carbon in austenite
$\bar{D}$	weighted average diffusivity of carbon in austenite
f_1	normalized supersaturation
H_1	kinetic function
J	diffusion flux
$\Delta L/L$	relative length change in dilatometry
$1/\bar{L}$	number of intercepts of austenite–ferrite interface per unit length of test line
M_s	martensite-start temperature
N_v	number of particles of austenite per unit volume
q	increase in the half-thickness of austenite
R	rate of carbon concentration dilution in austenite

6 J. R. Yang and H. K. D. H. Bhadeshia, in G. W. Lorimer (ed.), *Proc. Int. Conf. on Phase Transformations, 1987*, The Institute of Metals, London, 1988, pp. 203–206.
7 D. J. Sparkes, *Welding Inst. Res. Rep. 352/1987*, 1987 (The Welding Institute, Cambridge, U.K.).
8 N. C. Law and D. V. Edmonds, *Metall. Trans. A, 11* (1980) 33.
9 S. Matsuda and Y. Okamura, *Trans. Iron Steel Inst. Jpn., 14* (1974) 445.
10 H. K. D. H. Bhadeshia and L. E. Svensson, *J. of Mater. Sci.*, in the press.
11 L. E. Svensson and H. K. D. H. Bhadeshia, *Proc. Int. Conf. on Weld Quality and the Role of Computers*, Pergamon, Oxford, 1988, pp. 71–78.
12 R. Reed and H. K. D. H. Bhadeshia, *Int. Conf. on Trends in Welding Research*, Gatlingburg, to be presented in May, 1989.
13 H. K. D. H. Bhadeshia, in G. W. Lorimer (ed.), *Proc. Int. Conf., Phase Transformations 1987*, The Institute of Metals, London, 1988, pp. 309–314.
14 H. K. D. H. Bhadeshia and D. V. Edmonds, *Acta Metall., 28* (1980) 1265–1273.
15 J. R. Yang and H. K. D. H. Bhadeshia, in S. A. David (ed.), *Advances in the Science and Technology of Welding*, American Society for Metals, Metals Park, OH, 1987, pp. 187–191.
16 M. Strangwood and H. K. D. H. Bhadeshia, in S. A. David (ed.), *Advances in the Science and Technology of Welding*, ASM, Metals Park, OH, 1987, pp. 209–213.
17 J. W. Christian and D. V. Edmonds, in A. R. Marder and J. I. Goldstein (eds.), *Phase Transformations in Ferrous Alloys*, The Metallurgical Society of AIME, Warrendale, PA, 1984, pp. 293–326.
18 H. K. D. H. Bhadeshia, in H. I. Aaronson *et al.* (eds.), *Proc. Int. Conf. on Solid→Solid Phase Transformations*, The Metallurgical Society of AIME, Warrendale, PA, 1981, pp. 1041–1048.
19 M. Hillert, *Int. Rep., 1953* (Swedish Institute of Metals Research).
20 J. S. Kirkaldy, *Can. J. Phys., 36* (1958) 907.
21 G. R. Purdy, D. H. Weichert and J. S. Kirkaldy, *Trans. Metall. Soc. AIME, 230* (1964) 1025.
22 D. E. Coates, *Metall. Trans., 4* (1973) 2313.
23 H. K. D. H. Bhadeshia, *Prog. Mater. Sci., 29* (1985) 321–386.
24 A. Hultgren, *Jernkontorets Ann., 135* (1951) 403.
25 M. Hillert, *Jernkontorets Ann., 136* (1952) 25.
26 E. Rudberg, *Jernkontorets Ann., 136* (1952) 91.
27 H. I. Aaronson, H. A. Domian and G. M. Pound, *Trans. Metall. Soc. AIME, 236* (1966) 768.
28 J. W. Christian, *Theory of Transformations in Metals and Alloys*, Pergamon, Oxford, 2nd Edn., Part I, 1975.
29 R. T. DeHoff and F. N. Rhines (eds.), *Quantitative Microscopy*, McGraw-Hill, New York, 1968.
30 C. Zener, *J. Appl. Phys., 20* (1949) 950.
31 C. A. Dubé, *Ph.D. Thesis*, Carnegie Institute of Technology, 1948.
32 C. Atkinson, *Acta Metall., 15* (1967) 1207.
33 R. P. Smith, *J. Am. Chem. Soc., 68* (1946) 1163.
34 C. Wells, W. Batz and R. F. Mehl, *Trans. Metall. Soc. AIME, 188* (1950) 533.
35 R. H. Siller and R. B. McLellan, *Trans. Metall. Soc. AIME, 245* (1969) 697.
36 R. H. Siller and R. B. McLellan, *Metall. Trans., 1* (1970) 985.
37 H. K. D. H. Bhadeshia, *Met. Sci. J., 15* (1981) 477–479.
38 R. Trivedi and G. M. Pound, *J. Appl. Phys., 38* (1967) 3569.
39 H. K. D. H. Bhadeshia and A. R. Waugh, *Acta Metall., 30* (1982) 775–784.
40 A. Schrader and F. Wever, *Arch Eisenhuttenwes., 23* (1952) 489.
41 S. J. Matas and R. F. Hehemann, *Trans. Metall. Soc. AIME, 221* (1961) 179.
42 H. K. D. H. Bhadeshia, *Met. Sci. J., 16* (1982) 159–165.
43 H. K. D. H. Bhadeshia, *Scr. Metall., 22* (1988) I–IV.

Appendix A: nomenclature

$a_{\alpha F}$	lattice parameter of ferrite at any stage of reaustenitization
$a_{\alpha I}$	lattice parameter of ferrite at the beginning of reaustenitization
$\alpha_{\gamma F}$	lattice parameter of austenite at any stage of reaustenitization
$a_{\gamma I}$	lattice parameter of austenite at the beginning of reaustenitization
Δa_m	minimum detectable increase in austenite thickness
Ae_3	boundary separating the γ and $\alpha + \gamma$ phase fields
B_s	bainite-start temperature
c	initial length of ferrite plate
C^1	carbon concentration in the austenite before the start of reaustenitization
$C^{T_0'}$	carbon concentration given by the T_0 curve
C^γ	carbon concentration of residual austenite
$C^{\alpha\gamma}$	carbon concentration in ferrite which is in equilibrium with austenite
$C^{\gamma\alpha}$	carbon concentration in austenite which is in equilibrium with ferrite
CHT	continuous-heating transformation
D	diffusivity of carbon in austenite
$\bar{D}$	weighted average diffusivity of carbon in austenite
f_1	normalized supersaturation
H_1	kinetic function
J	diffusion flux
$\Delta L/L$	relative length change in dilatometry
$1/\bar{L}$	number of intercepts of austenite–ferrite interface per unit length of test line
M_s	martensite-start temperature
N_v	number of particles of austenite per unit volume
q	increase in the half-thickness of austenite
R	rate of carbon concentration dilution in austenite